continuously bubbled through the refluxing solution. This procedure eliminates the formation of chlorin contaminants. The solvent was then removed on a rotary evaporator, and the remaining thick purple oil was combined with 20 g of basic alumina. The porphyrin impregnated solid was placed in a Sohxlet extractor and extracted with methanol until the condensate was almost clear. This removes tarry impurities, but leaves the porphyrin bound to the silica since it is insoluble in methanol. Methylene chloride was then substituted for methanol, and the relatively pure porphyrin was washed off the support. After evaporation of the solvent, the porphyrin was chromatographed on neutral alumina (1:1 toluene/hexane eluant) and metallated by the literature procedure.[32]

Instrumentation. All proton NMR spectra were obtained on a Nicolet NMC 300 MHz spectrometer. Chemical shifts are reported relative to Me_4Si. ^2H NMR spectra were recorded on the same instrument operating at 46 MHz, employing the lock channel for signal observation. Chemical shifts are reported relative to $CDCl_3$ internal standard (7.25 ppm). Gas chromatographic analyses were performed on a Hewlett-Packard model 5880A gas chromatograph fitted with 12 ft × $^1/_8$ in. column of Chromasorb P.

Methods. The reaction conditions employed for the manganese porphyrin catalyzed epoxidation of olefins by lithium hypochlorite have been described previously.[10] The same reaction conditions were used for all experiments reported in this paper unless otherwise stated. All runs which were analyzed by NMR involved a modified workup. Once the oxygenation reaction had reached the desired conversion, stirring was stopped, and the organic layer removed by pipette. The solvent was evaporated, and approximately 5 mL of pentane added. This resulted in the precipitation of the porphyrin, the quaternary ammonium salt, and the axial ligand. The resulting mixture was filtered through a short plug of sand to remove insoluble material. The pentane was evaporated, yielding a mixture of the olefin(s) and oxygenated products. These were dissolved in the appropriate solvent and analyzed by NMR. This procedure avoids any fortuitous separation of products prior to analysis.

Iron-Porphyrin Catalyzed Reactions. F_5PhIO (0.24 mmol) was suspended in 500 μL of methylene chloride containing 0.5-1.0 mmol of substrate. Then 3.34×10^{-4} mmol of FePFPCl in 100 μL of methylene chloride was added. The reaction was allowed to proceed until all of the oxidant had disappeared. The solvent was then removed by rotary evaporation, and the product mixture dissolved in the appropriate solvent for NMR analysis.

Acknowledgment. We thank Dr. Scott A. Raybuck and Philip Hampton for assistance in the synthesis of FePFPCl. We also thank Dr. Lisa McElwee-White and Jeffrey Fitzgerald for helpful discussions. Financial support from the National Institutes of Health (Grant NIH GM17880-13,14) and the National Science Foundation (Grant NSF CHE83-18512) is gratefully acknowledged. The NMC-300 NMR spectrometer was purchased with funds from the National Science Foundation (Grant NSF CHE81-09064 to Stanford University).

Note Added in Proof. We have shown previously that both the manganese and iron porphyrin catalyzed reactions proceed through reversibly formed oxo-olefin intermediates.[10,15] This is assumed in the mechanistic arguments presented in this paper. Traylor and co-workers, however, have reported a kinetic study of an iron porphyrin catalyzed oxygenation reaction similar to the one discussed here and could find no evidence for an oxo-olefin intermediate.[16c] The major difference between our reaction conditions and those employed by Traylor's group is their addition of alcohol and water as co-solvents to solubilize pentafluoroiodosylbenzene. The *apparent* discrepancy between our results and Traylor's has been clarified recently in an elegant spectroscopic study by Groves and co-workers: Groves, J. T.; Watanabe, Y. *J. Am. Chem. Soc.* **1986**, *108*, 507-508. Their results are consistent with our kinetic study, as they are able to observe directly a high valent oxo-olefin complex which decomposes slowly to Fe^{III} porphyrin and epoxide. This species was formed by the addition of an olefin to an iron-oxo compound at -78 °C in methylene chloride. However, when alcohol was added to the preformed oxo-olefin complex, the intermediate immediately decayed to Fe^{III} and epoxide. How alcohols act to accelerate the decomposition of the high valent intermediate is an open question, but these experiments appear to provide a reconciliation between Traylor's kinetic studies and our own (see ref 16b).

Registry No. MnTPPCl, 32195-55-4; FeFPCl, 36965-71-6; $PhCH{=}CH_2$, 100-42-5; D_2, 7782-39-0.

A Photoelectron and Extended-Hückel Study of the Double-Metal-Layered Zirconium Monochloride, the Related Zirconium and Scandium Chloride Carbides M_2Cl_2C, and Their Relationship to Carbon-Centered Clusters

Robin P. Ziebarth, Shiou-Jyh Hwu, and John D. Corbett*

Contribution from the Department of Chemistry, Iowa State University, Ames, Iowa 50011.
Received August 12, 1985

Abstract: The bonding in the double-metal-layered ZrCl (AbcA), the hypothetical reordered ZrCl (AbaB), and the product of insertion of carbon into the latter to give M_2Cl_2C (Ab(c)aB), M = Zr, Sc, have been examined by photoelectron spectroscopy (UPS, XPS) and by extended-Hückel band calculations. The compounds characteristically exhibit well-resolved chlorine 3p and carbon 2p (when present) valence bands and a zirconium conduction band, with the substantial metal-nonmetal covalency in the first two bands. A significant amount of M-M bonding is contained within the carbon-binding states. The calculated density-of-states curves are in good agreement with UPS data for all three compounds in both energy and band shape, with the zirconium phases being metallic by both criteria. Bonding correlations between the known $Zr_6Cl_{12}C$-type clusters and the Zr_2Cl_2C condensation product of these are examined. The energies of the chlorine, carbon, and metal MO's (bands) in the two limits show a close correspondence in both experiment and theory. The orbital description of the relatively localized bonding of carbon within the Zr_6C cluster unit is also preserved on condensation. On the other hand, substantial delocalization leads to marked dispersion of the Zr-Zr bonding HOMO and LUMO cluster orbitals within the conduction band. Theoretical predictions of unknown derivatives of the title phases are also considered.

The zirconium monohalides ZrCl and ZrBr and the derivatives these form with a variety of nonmetals provide some novel and apparently unique bonding features that are relevant to the behavior of both metals and octahedral metal cluster compounds. The ZrX structures[1-3] consist of tightly bound infinite slabs containing four cubic-close-packed (ccp) layers sequenced X-Zr-Zr-X. A section of one slab is approximated by I although

(1) Adolphson, D. G.; Corbett, J. D. *Inorg. Chem.* **1976**, *15*, 1820.
(2) Troyanov, S. J. *Vestn. Mosk. Univ., Ser. 2: Khim.* **1973**, *28*, 369.

0002-7863/86/1508-2594$01.50/0

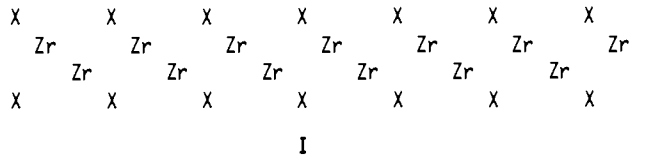

I

a common and more precise notation for the stacking order is (AbcA)[4] where the upper case letters denote halogen. These slabs are in turn held together by van der Waals forces much as are the more familiar CdX_2- and MoS_2-type layered structures. The details of the interslab ordering in all of these may result in several slabs per unit cell and polytypism is often found,[5] but none of this is particularly important relative to the present investigation of the strong interactions within the slabs. More importantly, the presence of the double-metal layers in the ZrX structures makes their properties and reactions quite different from those of the more classical layered materials that contain only single metal layers. The ZrX phases and their derivatives are appropriately intermediate both structurally and chemically between isolated clusters and the three-dimensional metal.

Three electrons per zirconium are delocalized in the intermetal region in the two ZrX phases, and the compounds are metallic according to both X-ray[3] (XPS) and UV[6] (UPS) photoemission spectral data and an earlier SCF-KKR band calculation.[7] The phases show an appropriate temperature-independent paramagnetism[7,8] and ZrCl, a conductivity parallel to the layers of ~ 55 ohm^{-1} cm^{-1}.[2] Numerous compounds can be formed through the binding of nonmetals in the nominal tetrahedral or octahedral holes between the pairs of zirconium layers either in the same ZrX structural arrangement or in one in which the close-packed layers are retained but repositioned in an hcp (AbaB) order. Most, if not all, of these are still metallic. Thus, oxygen atoms may be continuously added to 30–40% of the tetrahedral interstices in a ZrX matrix,[6] whereas rearrangement of the layers to an (AbaB) ordering occurs on bonding of B,[9] C, N,[10] and H[11] so that all the trigonal antiprismatic ("octahedral") sites between the double-metal layers (in layers positioned c) are occupied by the nonmetal, as in Zr_2Cl_2C, for instance. Both atom sizes and electronic factors are presumably responsible for the rearrangement of layers.

The synthetic results with the group 3 metals scandium and yttrium are similar for the carbides and nitrides of composition M_2Cl_2Z.[10] On the other hand, the parent phases "ScCl" and "YCl" evidently do not exist. Reported materials of this composition[12,13] turn out to actually be ternary examples of the foregoing kind, phases of the ZrX-type with a variable amount of hydrogen in the tetrahedral interstices.[14-16] The bonding in a phase such as Y_2Cl_2C is presumably quite similar to that in the zirconium analogue except that one fewer electron per metal makes it a nominal yttrium(III) compound and presumably a semiconductor. However, even this sort of conclusion is somewhat tentative when it is remembered that phases such as TiC and ZrC in the rock-salt structure are metallic owing to overlap of the otherwise filled valence and empty conduction bands.[17] In addition, the dark bronze to dark red-brown carbides M_2Cl_2C (M = Sc, Y, Zr) are generally obtained only as fine powders, making it difficult to establish the conduction properties of such anisotropic materials.

The present study was undertaken to examine the bonding properties of the ternary carbides Zr_2Cl_2C and Sc_2Cl_2C, since they are the best characterized, and to compare these results with the properties of the parent ZrCl. We have examined both the experimental density of photoionization states obtained by UPS techniques and the theoretical density of states estimated by extended-Hückel tight-binding calculations,[18] the latter program having been adapted and extended to meet the requirements of solid-state studies. A comparison of these two results also provides tests of two factors: (1) the extent to which we are able to categorize bulk electronic distributions by UPS, which is known to be surface sensitive and (2) the usefulness and credibility of calculational results achieved by this method for our purposes, namely, the identification and understanding of the important bonding characteristics of these extended solids as well as the determination of their probable metallic or semiconducting characters.

Simultaneous with the synthesis and structural characterization of the M_2X_2Z phases has been the discovery of a substantial collection of isolated M_6X_{12}-type clusters in which a variety of heteroelements may be bonded within the cluster, $Zr_6X_{14}C$ (X = Cl, I), $Zr_6Cl_{15}N$,[19,20] and $Sc(Sc_6Cl_{12}B)$[21] for example. Similar calculations and measurements are also available for some of these cluster phases.[9,20] This also provides the additional opportunity to compare the bonding properties of Zr_6C units in discrete clusters such as are found in $Zr_6Cl_{14}C$ with those in extended solids like Zr_2Cl_2C, the two structures being conceptually related by cluster condensation. Presumably at least the local bonding in these two circumstances should be very similar. It will be noted that Zr_2Cl_2C and $Zr_6Cl_{14}C$ are both formally zirconium(III) compounds so the comparison is not at all unreasonable from a chemical point of view.

Experimental Section

Materials. The synthesis and structural characterization of Zr_2Cl_2C and Sc_2Cl_2C samples that are single phase according to Guinier powder methods has been described elsewhere.[10] Briefly, these are obtained by reactions of stoichiometric amounts of powdered metal, the normal-valent chloride, and graphite at 850–950 °C in welded tantalum (for Zr) or niobium (for Sc) tubing for several days.

Photoelectron Spectra. The ultraviolet (UPS) data were secured with the aid of helium resonance radiation of 21.2 (I) or 40.8 (II) eV and an AEI model ES-200B instrument coupled with a Nicolet 1180 minicomputer for data averaging and curve smoothing. Generally, 2–11 scans were recorded in 512 channels, and the data were smoothed by a 9-point running average. Samples were opened in the helium-filled drybox (<1 ppm O_2, <0.5 ppm H_2O) that is attached directly to the sample port of the spectrometer: a sample was ground and pressed into thin indium foil on the probe, and this was immediately inserted into the spectrometer. Most of the compounds are metallic and give a clear edge at the Fermi level. The position of E_F is highly reproducible in the spectrometer output (±0.05 eV), and the scale has also been checked against the reported fine structure of gold in the 3–8 eV region.[22] The ability to generate fresh surface and to cover the indium relatively well with these layered compounds aids considerably in obtaining quality data. Experience has shown that spectra pertinent to the bulk phase rather than surface impurities may be consistently obtained under these circumstances.[22,23] The spectra generated with Al Kα radiation (1486.6 eV) were measured similarly except that these were referenced to the 1s level of adventitious carbon

(3) Daake, R. L.; Corbett, J. D. *Inorg. Chem.* **1977**, *26*, 2029.
(4) Hexagonal nets that are close-packed in any sequence are conventionally described in terms of A, B, or C representations of their relative orientation in projection. This description may also be used for interstitial atoms in tetrahedral, octahedral, or trigonal prismatic surroundings between the layers. The [110] sections of such structures are very convenient pictorials since all atoms lie on such planes.
(5) Hulliger, F. *Structural Chemistry of Layer-Type Phases*; Levy, F., Ed.; D. Reidel: Boston, 1976.
(6) Seaverson, L. M.; Corbett, J. D. *Inorg. Chem.* **1983**, *22*, 3202.
(7) Marchiando, J. F.; Harmon, B. N.; Liu, S. H. *Physica B + C: (Amsterdam)* **1980**, *99B*, 259.
(8) DiSalvo, F. J. personal communication, **1977**.
(9) Ziebarth, R. P.; Corbett, J. D., unpublished research.
(10) Hwu, S.-J.; Ziebarth, R. P.; Winbush, S. v.; Ford, J. E.; Corbett, J. D. *Inorg. Chem.* **1986**, *25*, 283.
(11) Wijeyesekera, S. D.; Corbett, J. D. *Solid State Commun.* **1985**, *54*, 657.
(12) Poeppelmeier, K. R.; Corbett, J. D. *Inorg. Chem.* **1977**, *16*, 1109.
(13) Mattausch, Hj.; Hendricks, J. B.; Eger, R.; Corbett, J. D.; Simon, A. *Inorg. Chem.* **1980**, *19*, 2128.
(14) Wijeyesekera, S. D.; Hwu, S.-J.; Corbett, J. D., submitted for publication.
(15) Simon, A.; Mattausch, Hj. personal communication, **1985**.
(16) Ueno, F.; Ziebeck, K.; Mattausch, Hj.; Simon, A. *Rev. Chim. Miner.* **1984**, *21*, 804.
(17) Schwarz, K.; Ripplinger, H.; Neckel, A. *Z. Phys. B: Condens. Matter* **1982**, *B48*, 79.
(18) Hoffmann, R. *J. Chem. Phys.* **1963**, *39*, 1397.
(19) Ziebarth, R. P.; Corbett, J. D. *J. Am. Chem. Soc.* **1985**, *107*, 4571.
(20) Smith, J. D.; Corbett, J. D. *J. Am. Chem. Soc.* **1985**, *107*, 5704.
(21) Hwu, S.-J.; Corbett, J. D., unpublished research.
(22) Corbett, J. D.; Marek, H. S. *Inorg. Chem.* **1983**, *22*, 3194.
(23) Corbett, J. D.; Meyer, G.; Anderegg, J. W. *Inorg. Chem.* **1984**, *23*, 2625.

at 285.0 eV. The core binding energy data for the same samples are reported elsewhere.[10]

Calculations. Two-dimensional, extended-Hückel band calculations have been carried out on the slab structures of ZrCl (AbcA), the hypothetical "ZrCl" (AbaB), i.e., Zr_2Cl_2C minus the carbon, Zr_2Cl_2C and Sc_2Cl_2C, each cell containing two metal and two chlorine atoms. The cluster condensation process was also considered, in this case for a quadrupled cell so that all "cluster" atoms were contained therein. The structural input involved the known lattice parameters, the experimental positional parameters for ZrCl and Sc_2Cl_2C, and atomic positions estimated for "ZrCl" and Zr_2Cl_2C on the basis of probable bond lengths, those for the last being based on extensive experience gained with carbon-centered zirconium cluster compounds.[19] The program utilized was one developed[18] and modified by Hoffmann and co-workers. The H_{ii} values for zirconium 4d, 5s, and 5p were obtained by linear interpolation between those deduced for Mo[24] and Y.[25] No data have been reported for scandium, and so these were approximated with the yttrium values. Standard values in the program package were used for carbon 2s and 2p and chlorine 3s and 3p orbitals. Orbital exponents and coefficients of the double-ζ expansion were as tabulated.[26] The positional, energy, and orbital parameters used are collected in the supplementary material. All overlap integrals were evaluated out to 9.9 Å, the remainder being set equal to zero. The density-of-states (DOS) curves were all calculated by using an evenly spaced, symmetry-weighted grid of 65 k points in the two-dimensional irreducible portion of the Brillouin zone except that the larger cluster fragment calculation utilized 5 k points. (The former calculations require about 25 min cpu time on a VAX 11/780.) The DOS curves were smoothed with Gaussian functions with a half-width of 0.1 eV at half maximum.

Results

Structural Relationships. An understanding of the results and their interrelationships first requires an appreciation of the structures of the phases studied and their differences. At the top of Figure 1 is shown an extended portion of the four-layer slab in ZrCl in which lines interconnect nearest neighbor zirconium atoms in the two central layers. A much more informative and terse description of the structural arrangements is accomplished with the [110] sections[4] shown in the lower part of Figure 1, where it is understood that the layers run horizontally, and the c axis is vertical. On the left in the figure is the AbcA (or ccp) representation of the layering in one slab of ZrCl and ZrBr (the complete description of these 3R-type structures involves three slabs) while on the right is that of the rearranged slab with heavy atoms ordered AbaB (or hcp) and the interstitial atom Z (carbon here) in relative position c, centered in a trigonal antiprism ("octahedron") of zirconium atoms. It will be immediately noted that this interstitial does not have any atoms above and below it, that is, out the triangular ends of the trigonal antiprism. This appears to be a fairly general geometric requirement for centered octahedra (except with H) whether these be isolated, in chains, or in sheets. The original ZrX arrangement does not allow this (Figure 1, left); with the interstitial atom at x the order would be Ab(a)cA, giving Cl–C–Cl strings parallel to the c axis. One rationalization of the instability of this structure is repulsion between the nonmetals so arrayed, about 2.92 Å apart in the hypothetical (Ab(a)cA) form of Zr_2Cl_2C. Of course, there may also be electronic reasons for the switch as well, as have been discerned when *two* hydrogens are placed in each trigonal antiprismatic cavity in 1T-ZrBrH rather than in tetrahedral holes in the 3R-structure.[14]

There is also a convenient connection between these layering alternates and the clusters from which they can be conceptually condensed. The ZrCl-type (AbcA) slab is achieved by condensing Zr_6Cl_8 (face-capped) clusters about the six Zr–Zr edges around the cluster waist of the Zr_6 octahedron, normal to a $\bar{3}$ axis, thereby eliminating six chlorines and retaining only the two that lie on the threefold axis so as to produce $^2_\infty[Zr_{6/3}Cl_2]$. On the other hand, Zr_6Cl_{12}-type (edge-bridged) clusters condensed in the same way retain six chlorines, the three lying over and outward from the edges of each triangular end of the metal antiprisms. Each chlorine now becomes shared with two other condensed clusters

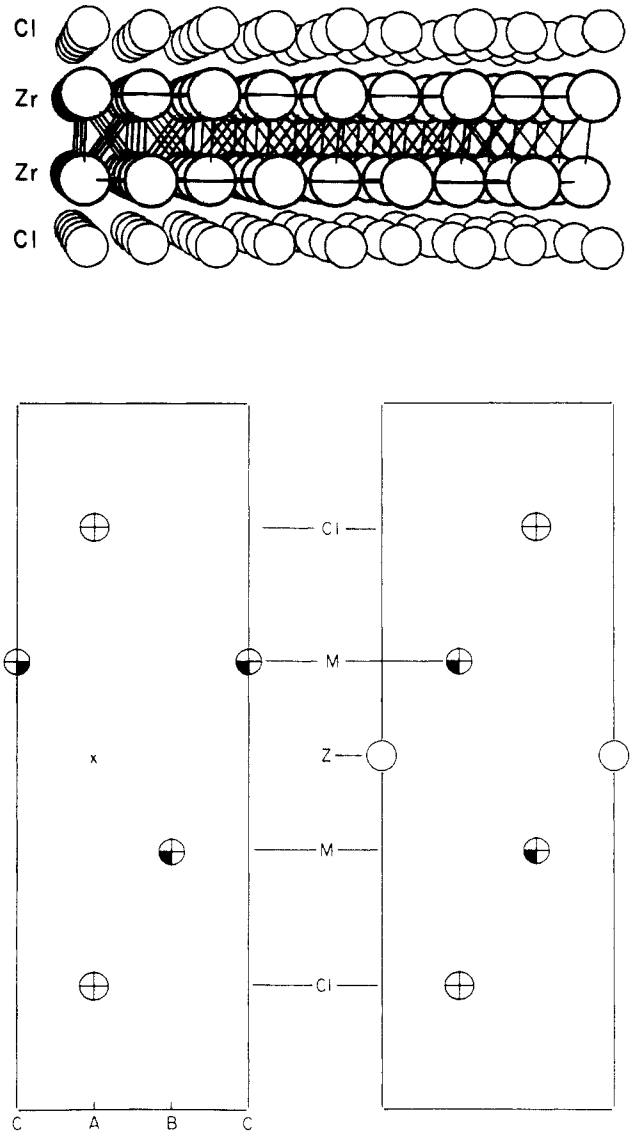

Figure 1. Top: a perspective view of a portion of a slab in the ZrCl and ZrBr structures with zirconium the larger, interconnected spheres. Bottom: the [110] section[4] for each slab in the ZrX structure (left) and in the 1T-structure of Zr_2Cl_2C (right). The layers are horizontal and the c-axis is vertical. The small × marks the trigonal antiprismatic site in ZrX. Crossed figures are chlorine, shaded ellipsoids are zirconium, and open circles are carbon.

to give the hypothetical $^2_\infty[Zr_{6/3}Cl_{6/3}]$ with (AbaB) ordering within the slabs.

In the following sections, the results of the band calculations for ZrCl, Zr_2Cl_2C, and Sc_2Cl_2C are presented and analyzed, and these are compared with the experimental results for all three as measured by ultraviolet photoelectron spectroscopy (UPS). The calculations were also carried out for "ZrCl", the hypothetical AbaB version which is the direct precursor to 1T-Zr_2Cl_2C, and for the condensation process described above that leads to Zr_2Cl_2C.

Zirconium Monochloride. The results from extended-Hückel calculations for the familiar ZrCl are shown in Figure 2 in terms of the total density-of-states (DOS) for valence levels down to −10 eV below E_F. Also included is the projection of the zirconium contribution to each band, chlorine making up the difference. The valence region can accordingly be described in terms of two bands at −(8.2–6.3) and −(2–0) eV which are mainly derived from chlorine and zirconium, respectively. Zirconium accounts for virtually all of the states in the higher lying conduction band, the lowest feature in this containing a significant Zr 5s contribution with the remainder being Zr 4d. Zirconium also makes a moderate contribution to the six low-lying "chlorine" bands which are seen here as a single composite "band". The zirconium involvement

(24) Hughbanks, T.; Hoffmann, R. J. *J. Am. Chem. Soc.* **1983**, *105*, 1150.
(25) Miller, G.; Burdett, J. personal communication, **1984**.
(26) Basch, H.; Gray, H. B. *Theor. Chim. Acta* **1966**, *4*, 367.

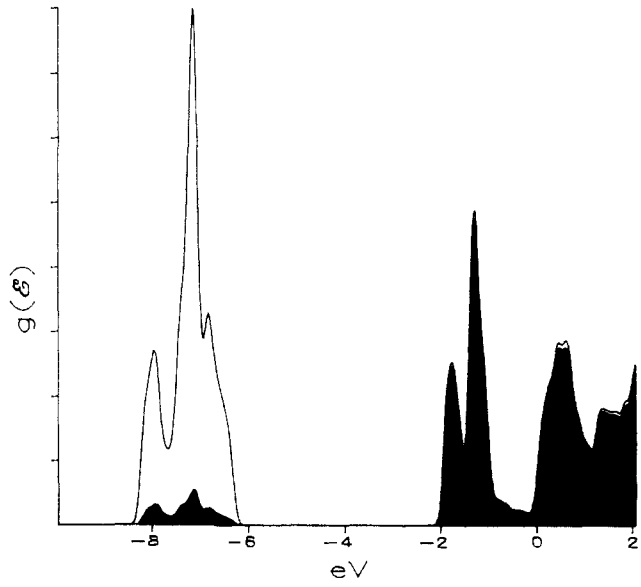

Figure 2. Total density of states g(E) for ZrCl (AbcA) vs. binding energy (eV) calculated by extended-Hückel methods (65 k points, E_F = 0). The shaded inset marks the projection of zirconium 4d (and 5s) contributions to the total DOS; chlorine 3p makes up the difference.

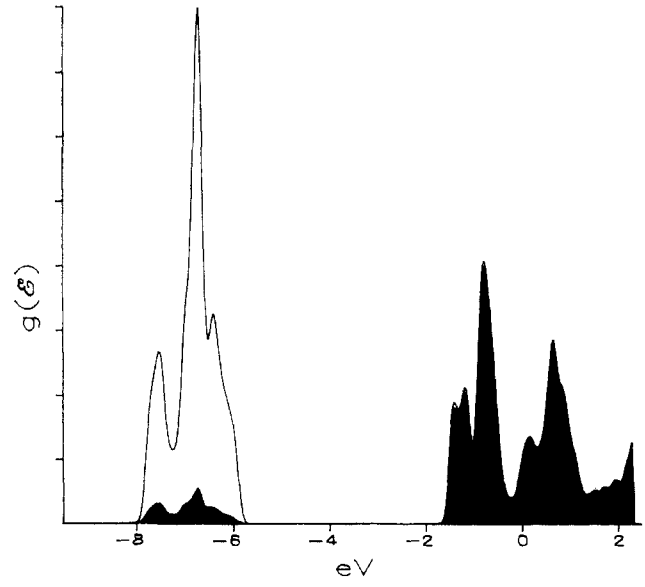

Figure 3. The total density of states calculated for the hypothetical hcp ZrCl (AbaB). The shaded inset gives the projection of zirconium 4d and 5s contributions to the total DOS.

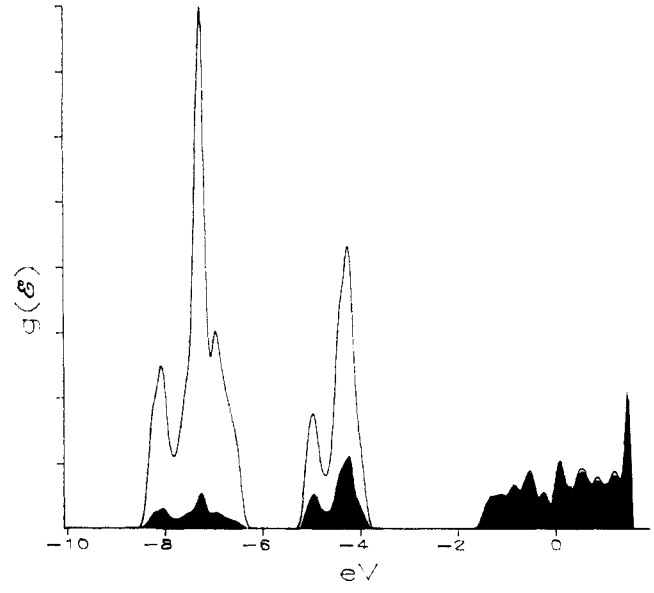

Figure 4. The total density of states vs. binding energy calculated for Zr_2Cl_2C by extended-Hückel methods (E_F = 0) and the projection of the zirconium contributions to the total DOS. Chlorine makes up substantially all of the difference in the first band (~−7 eV), and carbon does likewise in the middle band.

in this certainly represents the covalency of the outward-directed Zr–Cl bonds, a logical result since a low charge on chlorine would appear to be a prerequisite for the formation of a stable layered structure with a van der Waals gap between adjoining chlorine layers. The remainder of this large band consists of the chlorine contributions to the Zr–Cl bonds plus a larger number of essentially nonbonding but inseparable 3p functions on chlorine. The characteristically small mixing of metal and halogen is a result of both the structure and the sizable differences in valence energies of the orbitals for the two atoms, a feature that is in considerable contrast to the usual behavior of analogous sulfides, selenides, etc.[27,28]

Before considering the bonding in M_2Cl_2C, it is important to note again that the ZrCl matrix just considered is not that into which carbon is inserted, rather the relative orientation of the layers within each slab is altered from (AbcA) to (AbaB) (Figure 1). The corresponding DOS diagram for the hypothetical ZrCl with the same distances as in ZrCl but with (AbaB) packing (that is, of M_6X_{12} parentage) is shown in Figure 3. This is quite similar to that for the known structure, Figure 2, except that the lowest part of the unoccupied conduction band in ZrCl has broadened downward, and an extra feature very close to E_F has developed. These changes serve to drop E_F by ~0.5 eV, and the total energy achieved is also less by ~0.3 eV. While the numerical accuracy of the last is not high, a qualitative destabilization because of the reordering must be correct since the alternate structure has never been seen. According to overlap populations, the principal source of this stability loss is a decrease in Zr–Zr interlayer bonding on conversion from a M_6X_8– to a M_6X_{12}-type chlorine arrangement. This decrease is at least partially the result of the lessened participation of the zirconium $4d_{z^2}$ orbitals in interlayer bonding owing to their improved overlap with p_z orbitals on the second nearest neighbor chlorine in the same slab, viz., $\overset{\frown}{\text{Aba}}\underset{\smile}{\text{B}}$. There is also a smaller compensating increase in Zr–Zr intralayer bonding.

Zirconium Chloride Carbide. The corresponding calculation for Zr_2Cl_2C gives the valence DOS shown in Figure 4 together with lower-lying chlorine 3s and, mainly, carbon 2s bands at −22.5 and −14.7 eV, respectively. The projection of zirconium contributions on the total DOS is also shown in the figure. Again, the major atomic contributions to the bands allow ready assignment of these as chlorine 3p at ~−7 eV, carbon 2p at ~−4 eV, and zirconium 4d in the neighborhood of E_F. The zirconium components to these reflect the anticipated metal interactions, the binding of chlorine to the slabs as seen within the chlorine band (which also has a barely discernible carbon contribution, not shown), and a significant Zr–C (and Zr–Zr, see below) bonding in the carbon band. (There is only a very small chlorine component in the latter.) The effects of the Zr–C covalency are quite evident in the metal core (XPS) shifts as well.[10] The conduction band in Zr_2Cl_2C is again virtually pure zirconium in character. The lowest lying zirconium 5s contribution to the ZrCl conduction band in ZrCl has now disappeared into the carbon 2s and 2p bands, and some obviously necessary zirconium 4d states have also been pulled down from the conduction band into the carbon 2p band. This metal orbital redistribution will be returned to later.

A very useful comparison can be made between the calculated DOS curves for both ZrCl and Zr_2Cl_2C and the experimental densities of photoionization states determined with the aid of He I radiation. The latter represent the actual DOS's perturbed by relative cross sections for photoemission, which should be relatively

(27) Cisar, A. J.; Corbett, J. D.; Daake, R. L. *Inorg. Chem.* **1979**, *18*, 836.
(28) Corbett, J. D. *Adv. Chem. Ser.* **1980**, *186*, 329.

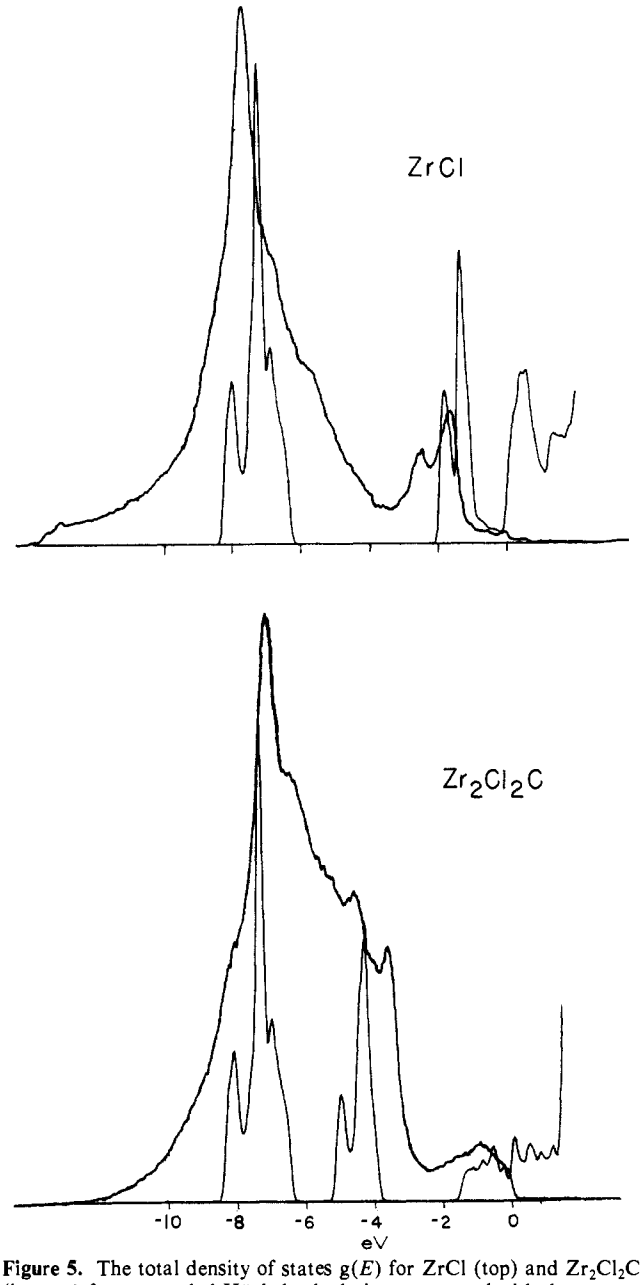

Figure 5. The total density of states g(E) for ZrCl (top) and Zr_2Cl_2C (bottom) from extended-Hückel calculations compared with the respective experimental spectra of photoemission states (He I, eV). The curves are superimposed at $E_F = 0$.

constant within each band. These comparisons are shown in Figure 5. The general agreement between theory and experiment for ZrCl (top) is pleasing, both as to the shape of the bands and energies, including the distinctive upturn in occupied states observed at E_F. An even better agreement in band energies could obviously be secured by adjusting the H_{ii} values by ~0.3 eV, but this "shoehorning" would serve little purpose. The results of a prior SCF-KKR calculation[7] for ZrCl agree fairly well with those from this simpler calculation in band shape and orbital contributions although the former predicted three rather than the two clear features observed for the zirconium band and did not achieve a very reasonable energy for the chlorine band, placing it at only −(3–6) eV. The low but finite DOS at E_F and, hence, the metallic behavior of ZrCl result from the degeneracy of the highest occupied and the lowest unoccupied bands at Γ (k = 0, 0) and their invariancy in z. The agreement between theory and experiment seen for Zr_2Cl_2C in the lower part of Figure 5 is exceptionally good, even as to the larger components of band shape, while the small differences in energies are again not significant. The metallic character of the Zr_2Cl_2C phase seems assured by the experimental

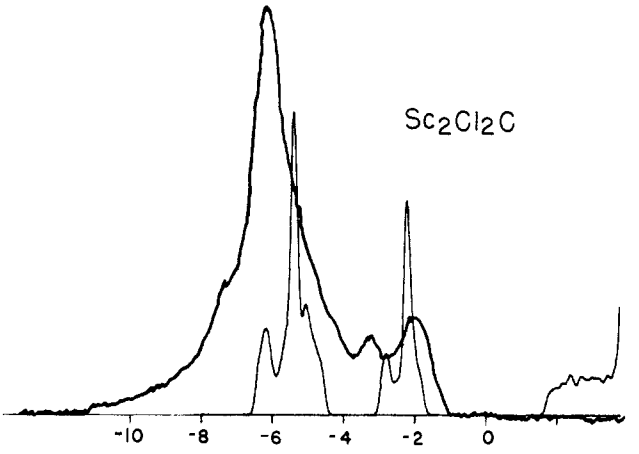

Figure 6. A total density of states for Sc_2Cl_2C calculated by extended-Hückel methods and the experimental photoemission spectrum (He I). The spectrum of the semiconducting Sc_2Cl_2C has been displaced to lower binding energies by 1 eV (see text).

spectrum as well as by theory. The UPS spectrum measured for Zr_2Br_2C also shows a similar conduction band with a pronounced Fermi edge and a more prominent carbon band owing to the relatively smaller cross section of the bromine 4p states.

The Fermi energy is found to move downward on formation of Zr_2Cl_2C from ZrCl (AbcA) if the chlorine bands in the UPS results are used as an internal reference. Most of this can be attributed to the loss of the very low DOS portion of the conduction band between 0 and about −0.7 eV in ZrCl (Figure 2). Stoichiometrically, the conduction band goes from three to one filled zirconium state per Zr_2Cl_2C in the process as $^4/_2$ electron pairs are removed into the new carbon 2s and 2p bands. Since four zirconium states per carbon are also needed for that purpose, some of these would appear to come from above E_F in ZrCl. The lowest energy feature in the ZrCl conduction band that involves a substantial metal 5s component is part of the zirconium involvement in the carbon 2s and 2p bands on carbide formation.

Scandium Chloride Carbide. As might be expected, the calculation for Sc_2Cl_2C provides little that is new in terms of the character of the chlorine and carbon bands, but the conduction band now lies well above these and is empty. The total DOS calculated again compares favorably with the UPS results for the 3R-polytype, as shown in Figure 6 with one alteration. This particular UV spectrum was rather well-resolved, and the sample gave exceptionally narrow and well-shaped core peaks as well. However, the result at face value indicates a 4-eV band gap if E_F is, as theoretically proper, located in the middle of the gap. This large a gap seems highly unlikely for a very dark red-brown phase and presumably arises because a real material with an appreciable electrical gap does not always adhere to the ideal E_F reference within the spectrometer. Charging may also be responsible. With these factors in mind, the experimental spectrum in Figure 6 has been shifted 1 eV to lower binding energies to give a more plausible 2-eV gap. Relative to the chlorine band, the carbon-based feature in Sc_2Cl_2C lies about 1 eV higher than in Zr_2Cl_2C, an appropriate shift considering the higher (less negative) orbital energies for a group 3 element.

Useful photoemission data have also been obtained for the zirconium and scandium chloride carbides utilizing harder radiation. Shown at the top of Figure 7 is the spectrum for Zr_2Cl_2C obtained with He II radiation (40.8 eV). At this energy the cross section of the chlorine 3p band is relatively smaller, and the carbon band in particular is much more evident. Plotted below this are the XPS valence spectra for Zr_2Cl_2C and Sc_2Cl_2C, respectively. These reflect, with the customarily lower resolution, the same qualitative features already seen with UV radiation for the higher lying valence levels, but in addition they also locate the chlorine 3s bands in Zr_2Cl_2C and Sc_2Cl_2C at −18.5 and −17.5 eV, respectively, compared with −17.7 eV in ZrCl[27] and the nominal carbon 2s valence bands at about −20.2 and −20.9 eV. (The results for Sc_2Cl_2C may be subject to the same referencing problem

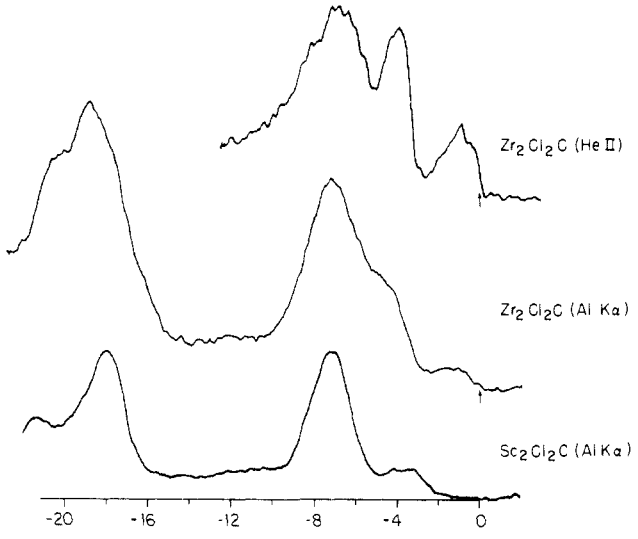

Figure 7. Top: the He II photoemission spectrum of Zr_2Cl_2C in the valence region. Middle and bottom: the XPS valence spectra (Al Kα) for Zr_2Cl_2C and Sc_2Cl_2C, respectively.

discussed above but probably to a different degree under X-ray (and electron) radiation. The core data[10] did not suggest charging was a problem.) There may have been some overlap in energy of the Cl 3s result in these two spectra with the composite In 4d emission from the substrate at −17.0 eV,[22] but in these particular cases the coverage of the foil was exceptionally good, and the indium core levels were observed to be quite weak. Broadening of the Cl 3s feature to lower energies is seen when greater amounts of indium show through. The observed chlorine 3s and carbon 2s levels in both are about 4 eV less negative and 6 eV more negative, respectively, than those calcualted. This is not a particularly surprising discrepancy as the H_{ii} input values used in the calculation are not apt to be very accurate or often tested.

The above favorable comparisons of UPS and extended-Hückel results give considerable encouragement to further applications of both techniques. It is very satisfying that so much credible information regarding bonding in new and novel structures can apparently be obtained relatively inexpensively by extended-Hückel methods. The UPS method, which is notoriously surface sensitive, does in our experience provide information on bulk valence properties, especially (but not only) for layered materials where fresh surface can be easily created during mounting. At the same time we would be reluctant to make too much out of any features on the lower-lying parts of the chlorine bands. Preferred orientation of the mounted samples and a directional dependence of the emission from these layered materials were certainly present, but these were observed mainly to cause changes in the relative heights of different bands when the sample probe was rotated.

Figure 8 shows the so-called COOP (crystal orbital overlap population[29]) curves for Zr_2Cl_2C, these being overlap-weighted DOS curves for various pairs of atoms. Such data give a good representation of the bonding and antibonding contributions to various bands, occupied or not. For Zr_2Cl_2C these show that there are negligible Zr–Zr and Zr–C bonding components in the chlorine band, major Zr–C and significant Zr–Zr bonding, both interlayer and intralayer, in the "carbide" band, and mainly these two Zr–Zr components in the conduction band. The Zr–C values in the conduction band (not shown) are negative but less than that shown for Zr–Cl until all turn strongly antibonding beyond 1.5 eV.

It is important to note that substantial Zr–Zr bonding is also provided by states within the carbon band just as they are in the more localized t_{1u}^6 (metal plus carbon 2p) MO's in the isolated cluster.[20] In terms of overlap populations, Zr_2Cl_2C which formally contains d^1 zirconium(III) retains 30% of the Zr–Zr interlayer bonding and 23% of the intralayer bonding that was present in the carbon-free "ZrCl" (d^3, AbaB), slightly less of the interlayer

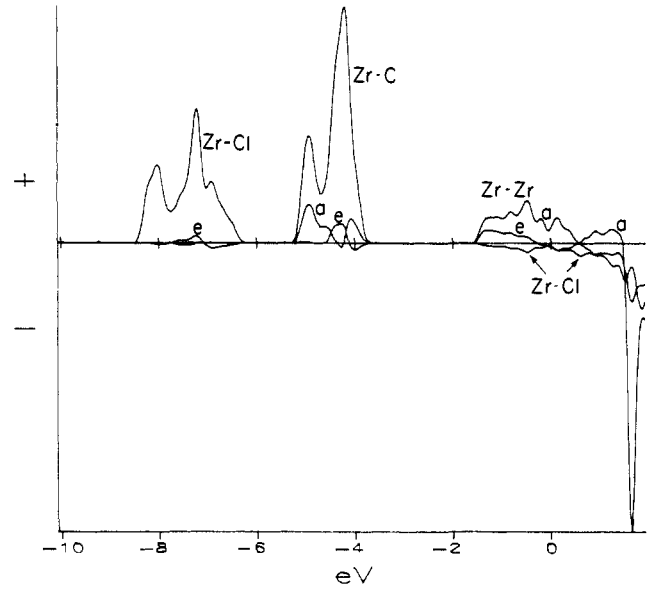

Figure 8. COOP curves for Zr_2Cl_2C labeled according to bonding contributions of different atom pairs: Zr–Zr intralayer (a), Zr–Zr interlayer (e), Zr–Cl (bands 1 and 3), and Zr–C (band 2). Other contributions are small. A positive sign denotes bonding.

metal bonding if the less related but "real" ZrCl is used for comparison. This loss is more than compensated for by very strong Zr–C bonding. According to overlap populations, 39% of the interlayer and 46% of the intralayer Zr–Zr bonding left in Zr_2Cl_2C occurs in the so-called carbide states around −4.0 eV. This provides a striking fact: that the total Zr–Zr bonding in Zr_2Cl_2C is 79% greater than inferred from only the zirconium(III) state and the Zr–Zr overlap population of the conduction band! Likewise, Sc_2Cl_2C (d^0 scandium(III)) still contains significant metal–metal bonding.

Predictions. The character of the COOP curves in Figure 8 in the neighborhood of E_F provides information as to whether conceivable electronic changes are favored or disfavored based on the assumption of a rigid band. In principle, this allows predictions to be made regarding conceivable chemical changes in or reactions of the layered substrates. In the case of Zr_2Cl_2C, the position of E_F and, thence, the bonding could be altered either by cation intercalation between the chlorine layers, with a corresponding reduction of the slabs and an increase in E_F, or through a change in the identity of the interstitial atom. According to Figure 8, Zr–Zr bonding states are clearly available just above E_F, and the optimum overlap would appear to be reached with about one more electron per Zr_2Cl_2C (+0.51 eV). This suggests that intercalation with an alkali metal to give $M^1Zr_2Cl_2C$ should be electronically favorable as far as the bonding within the slabs is concerned, yet all attempts to obtain such phases have resulted in decomposition (or no reaction). The same prospect applies to Sc_2Cl_2C (except that the gap must be surmounted) and, unfortunately, the same result as well.[10] On the other hand, Ta_2S_2C, which is isostructural and isovalent with Zr_2Cl_2C and which should have a similar band structure, has been intercalated with all of the alkali metals.[30] Furthermore, the compound Zr_2Cl_2N with one more valence electron than the carbide has been prepared, and the contraction seen in both the *a* and *c* lattice dimensions relative to the carbide presumably reflects both the smaller size of nitrogen and the addition of an electron to Zr–Zr bonding levels.[10,31]

The analogous COOP curves for ZrCl (not shown) also exhibit Zr–Zr bonding to beyond +0.5 eV, yet attempts at its intercalation continue to be unsuccessful[3,6,10] even though the Fermi level for a rigid structure would be only +0.26 eV for $M^1_{0.5}ZrCl$. The same

(29) Hughbanks, T.; Hoffmann, R. *J. Am. Chem. Soc.* **1983**, *105*, 3531.

(30) Brec, R.; Ritsma, J.; Ouvard, G.; Rouxel, J. *Inorg. Chem.* **1977**, *16*, 660.

(31) The corresponding boride appears to have been obtained too although it is not clear that the B–C–N series is uniform.[9]

pertains to the formation of NbCl in the ZrX structure (E_F = +0.44 eV) where a number of synthetic attempts have all failed, including some of "brute force" character. Presumably these all reflect what cannot be easily assessed theoretically, the thermodynamic stability of alternate zirconium phases, namely, MCl, ZrC, and ZrCl, instead of intercalated Zr_2Cl_2C and MCl, ZrCl and Zr rather than M^1_xZrCl. Phase stability remains a major problem in predicting solid-state chemistry.

Discussion

The collection of valence spectra and calculations already presented together with either or both types of data for nonmetal-centered Zr_6X_{12}-type clusters (X = Cl, I),[9,20] the metal chain compounds Sc_4Cl_6B and Sc_5Cl_8C,[21] and the related double-metal-layered $ZrXH_{0.5}$, ZrXH (X = Cl, Br), and $YClH_x$[14,22] show a remarkable commonality when viewed collectively from some distance. The general features are (a) a low-lying halogen p band (or MO) with a moderate metal contribution that originates from covalent bonding of the sheathing halogen to the metal framework, (b) an intermediate band (MO) for the interstitial atom that also contains a substantial metal component, and (c) a high-lying conduction band (MO) that is almost solely metal–metal bonding in character. The first and last features are also readily recognized in valence XPS and UPS data for a series of binary $ZrCl_n$ phases.[32,33] The character of these band results is in general not unusual for solids, but the collection exhibits remarkably similar features for a wide collection of metal-rich halide structures and bonding arrangements preselected for their stability and frequently exhibiting considerable structural novelty. Some common structural and bonding features have already been noted: an evidently dominant metal–metal (and, where appropriate, metal–interstitial) bonded framework with metal-like characteristics of high coordination number, longer M–M distances, and lower M–M bond orders; a metal arrangement that is inevitably based on condensed M_6X_8- or, more often, M_6X_{12}-type clusters, particularly when interstitials are involved; the importance of bonding of halogen at all metal vertices; the lack of screening (lengthening) of M–X distances by metal-bonding electrons; and, as so evident in the results presented here, the low contribution of halogen orbitals to the metal-based conduction band.[28,34]

Cluster Condensation. The condensation of M_6X_{12}-type clusters into extended M–M bonded arrays has proven to be a useful and a convenient conceptual basis for describing and interrelating the structures of many of the highly reduced rare-earth and transition-metal halides.[35-38] Furthermore, the characteristic descriptions of the extended bonding within the above infinite sheet or chain structures are in some respects not significantly different from the more familiar terms employed for isolated molecular-like clusters. In fact, there are many semiquantitative features to demonstrate that the local character of bonding between carbon and zirconium in Zr_2Cl_2C is quite similar to that in a variety of known phases containing $Zr_6X_{12}C$-type clusters, X = Cl, I, for which calculations and UPS data are also available.[9,19,20] The most studied among the latter are $Zr_6X_{14}C$ compositions, predominant phases that contain isolated carbon-centered $Zr_6X_{12}^{2+}$ clusters together with two additional halogen atoms that bridge between clusters. (Coincidentally, the zirconium oxidation state is 3+ in both Zr_2Cl_2C and in $Zr_6Cl_{14}C$.) The bonding in the octahedral cluster can be described in fairly familiar terms—the overlap of carbon s and p valence orbitals with Zr–Zr bonding orbitals of the same symmetry within the cluster to produce low-lying bonding states (a_{1g}^2, t_{1u}^6) while an unperturbed t_{2g}^6 HOMO level is Zr–Zr bonding in character.

The comparison between clusters and solids will be made on two bases, the relative bond (band) energies and the electronic

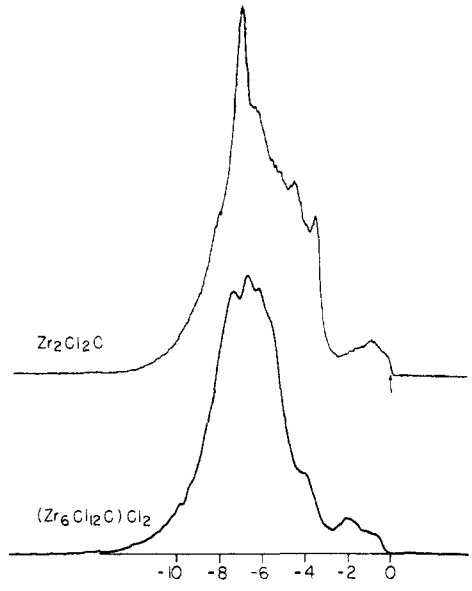

Figure 9. The He I photoemission spectrum of Zr_2Cl_2C (top) compared with that of $(Zr_6Cl_{12}C)Cl_2$ (bottom) (E_F = 0).

redistribution that takes place on their interconversion. A remarkably close correspondence in "band" energies is found when Zr_2Cl_2C and $Zr_6Cl_{12}C^{2+}$ are compared according to either theory or experiment. The calculations for the cluster[9,39] naturally yield discrete energies for the three levels mentioned above, and the experimental measurements would normally be referenced to a Fermi zero midway between the HOMO and LUMO (a_{2u}) cluster bands (MO's). If the data for $Zr_6Cl_{12}C^{2+}$ are instead referenced to the calculated HOMO level, the binding energies for the foregoing MO's in the cluster are 0, −4.0, and −6.8 eV for the zirconium, "carbon 2p", and "chlorine 3p" "bands", respectively, which compare well with about −0.7, −4.5, and −7.4 eV for the calculated band centers in Zr_2Cl_2C (Figure 4). The close correspondence is further emphasized in the comparison of experimental UV photoemission data for Zr_2Cl_2C and $Zr_6Cl_{14}C$[9] shown in Figure 9. The comparison is, of course, skewed by the markedly higher chlorine and lower carbon content in the cluster phase. Notwithstanding, there is clearly a considerable similarity in the energy of bands within a solid containing isolated clusters and those in an extended solid which consists of condensed clusters. The theoretical consideration of the latter is, of course, more complex because of the need to consider energies over a range of points in reciprocal (k) space. Electronic aspects of this process will be considered shortly.

Actually, much of the similarity should not be surprising. The Zr–C distances are nearly the same, the symmetries of the Zr_6C groups are similar (squashed D_{3d} vs. O_h), and the chlorines in the solid, though fewer in number, occur in bridging positions similar to half of those in the cluster. These and the applicability of virtually the same H_{ii} values for Zr, Cl, and C in both compounds would appear to ensure that the resultant energies will be very similar. The broadening found in the extended Zr_2Cl_2C solid is a result of dispersion of the energy bands within the Brillouin zone, but these bands are still rather flat in ZrCl,[7] as is also reflected in the relative narrowness of the observed UPS bands. Certainly the weakly coupled clusters in $Zr_6Cl_{14}C$ should give flat and narrow bands in k and in energy space as well. Thus, the major energy features of bonding in the infinite solid state appear neither mysterious nor unusual under these circumstances.

The extent to which cluster condensation ideas can be carried over and applied to the relationships between the electronic structures of isolated clusters and the resultant chains or the more

(32) Corbett, J. D.; Anderegg, J. W. *Inorg. Chem.* **1980**, *19*, 3822.
(33) The Fermi levels were incorrectly assigned in ref 29; see ref 6 and 22.
(34) Corbett, J. D., unpublished results.
(35) Simon, A *Chem. Unserer Zeit.* **1976**, *10*, 1.
(36) Poeppelmeier, K. P.; Corbett, J. D. *Inorg. Chem.* **1977**, *16*, 1107.
(37) Poeppelmeier, K. P.; Corbett, J. D. *J. Am. Chem. Soc.* **1978**, *100*, 5039.
(38) Simon, A. *Angew, Chem., Int. Ed. Engl.* **1981**, *20*, 1.

(39) Terminal halides from some source are bonded to the metal vertices in all structures of cluster compounds formed by metals from transition groups 3–6. Their presence is accordingly found to have a significant effect on bonding within the clusters,[20] and calculations are, therefore, best carried out on the corresponding $(M_6X_{12}Z)X_6$ groups.

condensed double-metal-layered structures has largely been neglected, perhaps with reason since some of the electronic effects turn out to be substantial. One of the major problems associated with the tracing of the MO's in an isolated cluster into a condensed array is the choice of a suitable building block to follow. Condensation of M_6X_{12} clusters into a two-dimensional ZrX-type sheet involves initial loss of six X atoms around the waist to give an M_6X_6 unit, followed by condensation along all of the exposed edges that have a component parallel to the $\bar{3}$ axis. Each element in the process becomes shared by three such condensed units, viz. $^2_\infty[Zr_{6/3}Cl_{6/3}]$.

Previous work regarding the electronic similarities between isolated clusters and solids has pertained to such as Mo_6S_8 clusters which condense into solid Mo_6S_8 with no loss of atoms during the condensation process and with only a small metal–metal interaction between neighboring cluster units so that the cluster MO's carry over into the solid with very little perturbation.[24] On the other hand, the condensation of Nb_6O_{12} clusters to form NbO involves sharing of all of the vertices of the metal octahedra as well as the bridging oxygen atoms and, hence, a much greater interaction between neighboring clusters, and only limited retention of the electronic structure of the isolated cluster is found.[40] Nearly all of the Nb–Nb bonding orbitals show a substantial broadening in the solid except for the a_{2u} cluster LUMO which is only mildly perturbed. On the whole, the cluster analogy appears to have some merit in cases where there is a large degree of localized bonding, as with the Mo_6S_8 example or the M–C bonding in the monocarbides.[41] In other cases where the bonding is largely delocalized, the electronic relationship between the isolated cluster and a condensed array appears to be much more tenuous. With these observations in mind, we have proceeded to analyze the electronic structure of Zr_2Cl_2C in terms of isolated Zr_6Cl_{12} cluster units, the results showing some of both of the characteristics just described.

The condensation of isolated $Zr_6Cl_{12}C$-type clusters into the extended sheet structure Zr_2Cl_2C starts first with the electronically more appropriate[39] $(Zr_6Cl_{12}C)Cl_6^{4-}$ unit with chlorine atoms terminal to each metal vertex. The condensation will be accomplished in a three-step process: compression of the metal octahedron along a $\bar{3}$ axis and elongation normal to this to give D_{3d} symmetry with no change in Zr–C or Zr–Cl distances, the loss of six terminal and six waist chlorine atoms to give a Zr_6Cl_6C unit, and, finally, condensation of this precursor into the infinite double-metal sheet structure. This process is depicted in Figure 10.

Of particular interest for our purposes are the Zr–C cluster bonding orbitals (a_{1g}, t_{1u}) and the Zr–Zr bonding orbitals near the Fermi energy (t_{2g}, HOMO and a_{2u}, LUMO). Compression of the $Zr_6Cl_{18}C$ clusters along a $\bar{3}$ axis simply splits the t_{1u} and t_{2g} sets in O_h symmetry into the corresponding $a_{2u} + e_u$ and $a_{1g} + e_g$ sets in D_{3d} symmetry while the a_{1g} and a_{2u} orbitals remain identical. Although the distortion of the octahedron is quite large (±5% in Zr–Zr distances), the orbital splitting caused is only on the order of 0.25 eV. The second process of ligand removal is more complicated. The loss of the six terminal atoms from an M_6X_{18} cluster has been previously examined.[20] To summarize briefly, when six Zr–Cl bonding orbitals as well as the 18 lone pairs (3s and 3p) associated with the terminal chlorine atoms are removed, what were formerly six Zr–Cl antibonding orbitals become essentially nonbonding metal orbitals above E_F, and the M–M bonding a_{1g} orbital is slightly stabilized by rehybridization. In the carbon-centered cluster, the rehybridization of the a_{1g} orbital is undoubtedly quite small because of the very large carbon 2s contribution. Loss of the six waist Cl atoms proceeds similarly; eighteen chlorine lone pairs and six Zr–Cl bonding orbitals and electron pairs are removed, leaving once again six nonbonding metal levels just above the Fermi energy. Thus, in spite of the harsh treatment of the $Zr_6Cl_{18}C$ cluster, including removal of nearly half of its atoms, all of the cluster MO's below E_F remain

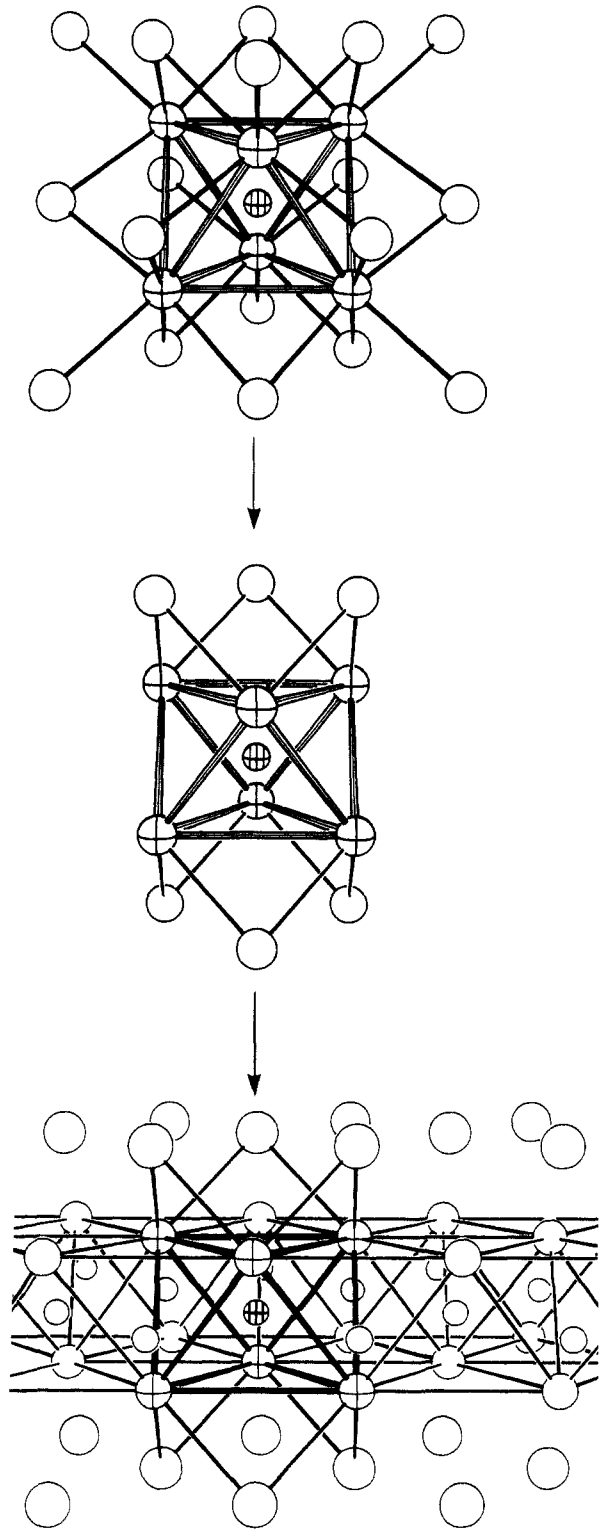

Figure 10. The condensation process from a $(Zr_6Cl_{12}C)Cl_6$ cluster through a Zr_6Cl_6C intermediate to the infinite layered Zr_2Cl_2C.

essentially unchanged except, of course, for those removed entirely because of ligand extraction.[42] In addition, the $Zr_6Cl_{18}C$ cluster LUMO a_{2u} remains the LUMO in the Zr_6Cl_6C fragment although it drops nearly 1.4 eV, primarily because of a reduction in Zr–Cl antibonding contributions resulting from the loss of the six chlorine atoms about the waist.

The transformation of Zr_6Cl_6C cluster MO's to the solid was followed by projecting out from the total DOS the charge density

(40) Burdett, J. K.; Hughbanks, T. *J. Am. Chem. Soc.* **1984**, *106*, 3101.
(41) Wijeyesekera, S.; Hoffmann, R. *Organometallics* **1984**, *3*, 949.

(42) The limit to this ligand removal, the nonmetal-centered naked metal cluster, is the one employed for bonding calculations by Lauher (Lauher J. W. *J. Am. Chem. Soc.* **1978**, *100*, 5305).

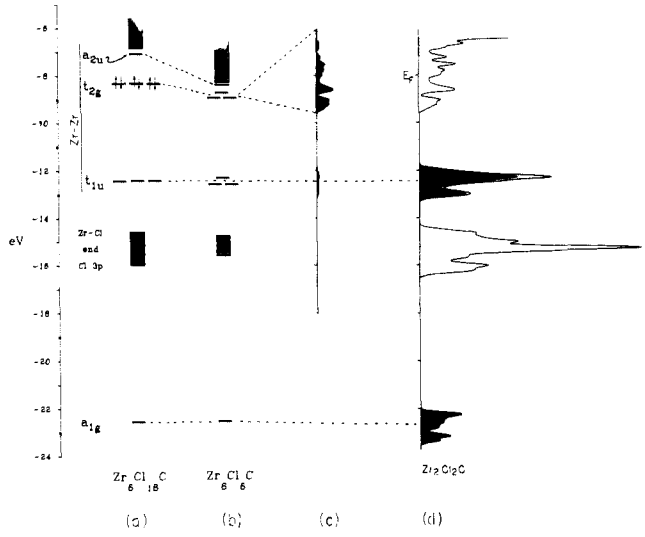

Figure 11. The changes in energies and electronic structure occurring during the transformation of the isolated cluster to the condensed solid. From left to right: (a) the MO diagram for $Zr_6Cl_{18}C^{4-}$ (O_h), (b) MO diagram for Zr_6Cl_6C (D_{3d}), (c) projection of the cluster t_{2g} (HOMO) orbital from the DOS of Zr_2Cl_2C (arbitrary scale), and (d) total DOS for Zr_2Cl_2C (condensation calculation). The contribution of the cluster Zr–C bonding orbitals a_{1g} and t_{1u} to the DOS in Zr_2Cl_2C is shown in black in part d.

Table I. Correlation of Zr_6Cl_6C Cluster MO's with the Corresponding Bands in Zr_2Cl_2C

Zr_6Cl_6C cluster orbtl (princpl charctr)	% of cluster orbtl found in equiv band in Zr_2Cl_2C
a_{1g} (C 2s)	100% (C 2s band)
e_u (C 2p) a_{2u}	98% 99% (C 2p band)
e_g	61%
a_{1g} (HOMO) (Zr–Zr)	37% Zr 4d band below E_F
a_{2u} (LUMO)	27%

for linear combinations of atomic orbitals corresponding to the MO's of interest in the Zr_6Cl_6C fragment. In other words, the MO's of the Zr_6Cl_6C cluster were used as a basis set for the crystal orbitals at each k point, thereby allowing the cluster MO contributions to each crystal orbital to be ascertained. The energetic changes that occur along the designed cluster condensation process are depicted in Figure 11 together with the projection of cluster-like orbitals in the solid, and numerical data regarding the cluster orbital-band distributions are given in Table I.

The results of our "cluster analysis" of Zr_2Cl_2C are not completely unexpected. The more localized Zr–C bonding orbitals (a_{1g}, e_u, and a_{2u}) in the cluster carry over into the solid virtually unaffected. The a_{1g} cluster orbital, largely carbon 2s in character, makes up the entirety of the carbon 2s band in Zr_2Cl_2C while the e_u and a_{2u} orbitals (Zr–C bonding) make up over 98% of the "carbon 2p" band, as shown. Simply stated, the Zr–C bonding in the condensed cluster array of Zr_2Cl_2C is largely localized and essentially identical with that in the isolated cluster. Similar statements have been made concerning the relationship between transition-metal carbides and carbon-centered clusters.[41] On the other hand, the cluster Zr–Zr bonding orbitals become much more widely dispersed because of the extensive Zr–Zr bonding with neighboring metal atoms, and the resultant delocalization that occurs on condensation as their like atom nearest neighbor coordination goes from four to nine. The extent to which the localized M–M cluster bonding character is lost upon cluster condensation is reflected in the fact that only ~50% of the cluster e_g and a_{2g} (~t_{2g}) orbitals can be traced to states in the zirconium 4d conduction band below the Fermi energy. If the M–M bonding in the solids were adequately represented just by that of the isolated cluster, nearly all of the conduction band states below E_F would be made up of these cluster orbitals. The remaining half of the states actually present are derived from MO's that lie above the Fermi energy in Zr_6Cl_6C, many being related to the zirconium nonbonding orbitals in the cluster formed during ligand extraction that now strongly participate in bonding to neighboring cluster units in the extended structure.

Cluster condensation is one of the most useful organizational concepts that have been applied to the growing array of highly reduced halides, sulfides, and oxides of the earlier transition metals that exhibit strong, extended metal–metal bonding in chains and sheets, namely the large fraction that can be described as having been derived from M_6X_{12}- or M_6X_8-type clusters. In the simplest case of chain formation, this process is envisioned to take place through sharing of trans edges of the metal octahedra and, sometimes, of adjoining nonmetals as well. In some cases cis edges of the cluster chains are also shared to gain double chains. In the mind's eye, continuation of the latter mode can be seen to generate ZrX-type sheets and, in principle, in the third dimension as well to approach the close-packed metal. Another mode found in Chevrel-like phases involves confacial condensation of M_6X_8 units into chains or segments. As useful as these pictures may be geometrically, the present approximations make clear that only very limited electronic insights can be gained from this approach when additional metal–metal bonds, extended bonding, and, therefore, bands are formed in ZrX-type sheets. Similar conclusions can be expected for chains, viz. Sc_4Cl_6B from $Sc(Sc_6Cl_{12}B)$,[21] and the same problems have been shown to pertain to the three-dimensional example NbO. Only localized bonding to an interstitial seems to carry an electronic fingerprint through the process, although this may not apply so well with closer interstitials in tetrahedral sites or on confacial condensation. Many interesting bonding questions regarding the condensed structures themselves still remain, including the considerable contrasts in compound and structure types found among the halides, oxides, and heavier chalcogenides.[43,44]

Acknowledgment. The calculations would not have been possible without the expert advice and assistance of Dr. Sunil Wijeyesekera. The PES data were ably measured by J. W. Anderegg. This research was supported in part by the National Science Foundation—Solid State Chemistry via grant DMR-8318616; R. P. Ziebarth was also the holder of Proctor and Gamble and Gilman Fellowships.

Registry No. ZrCl, 14989-34-5; Zr_2Cl_2C, 99665-57-3; Sc_2Cl_2C, 97005-30-6.

Supplementary Material Available: The atom positional, energy, and orbital parameters used in the calculations (2 pages). Ordering information is given on any current masthead page.

(43) Corbett, J. D. *Pure Appl. Chem.* **1984**, *56*, 1527.
(44) Corbett, J. D.; McCarley, R. E. In *Crystal Chemistry and Properties of Materials with Quasi-One-Dimensional Structures*; Rouxel, J., Ed.; D. Reidel: Dordrecht, Holland, in press.